Keratin8 Deficiency Aggravates Retinal Ganglion Cell Damage Under Acute Ocular Hypertension

Chengshou Zhang,[1] Naiji Yu,[1] Qiyu Qin,[1] Xingdi Wu,[1] Yuxiang Gu,[2] Tong Liu,[1] Qi Zhang,[1] Xin Liu,[1] Min Chen,[1] and Kaijun Wang[1]

[1]Eye Center, The Second Affiliated Hospital, School of Medicine, Zhejiang University, Zhejiang Provincial Key Laboratory of Ophthalmology, Zhejiang Provincial Clinical Research Center for Eye Diseases, Zhejiang Provincial Engineering Institute on Eye Diseases, Hangzhou, Zhejiang, China
[2]Department of Ophthalmology, The First People's Hospital of Xiaoshan District, Hangzhou, Zhejiang Province, China

Correspondences: Kaijun Wang and Min Chen, Eye Center, The Second Affiliated Hospital, School of Medicine, Zhejiang University, Zhejiang Provincial Key Laboratory of Ophthalmology, Zhejiang Provincial Clinical Research Center for Eye Diseases, Zhejiang Provincial Engineering Institute on Eye Diseases, 88 Jiefang Road, Shangcheng District, Hangzhou, Zhejiang 310009, China; ze_wkj@zju.edu.cn and chenmineye@zju.edu.cn.

CZ, NY and QQ contributed equally to this work.

Received: April 2, 2023
Accepted: August 3, 2023
Published: September 1, 2023

Citation: Zhang C, Yu N, Qin Q, et al. Keratin8 deficiency aggravates retinal ganglion cell damage under acute ocular hypertension. *Invest Ophthalmol Vis Sci.* 2023;64(12):1. https://doi.org/10.1167/iovs.64.12.1

Purpose. Keratin 8/18 (KRT8/18), paired members of the intermediate filament family, have shown vital functions in regulating physiological activities more than supporting the mechanic strength for cells and organelles. However, the KRT8/18 presence in retinal ganglion cells (RGCs) and functions on neuroprotection in a mouse model of acute ocular hypertension (AOH) are unknown and worthy of exploration.

Methods. We identified the existence of KRT8/18 in normal human and mouse retinas and primary RGCs. KRT8/18 levels were detected after AOH modeling. The adeno-associated virus (AAV) system was intravitreally used for selective KRT8 knockdown in RGCs. The histological changes, the loss and dysfunction of RGCs, and the gliosis in retinas were detected. The markers of cell apoptosis and MAPK pathways were investigated.

Results. KRT8/18 existed in all retinal layers and was highly expressed in RGCs, and they increased after AOH induction. The KRT8 knockdown in RGCs caused no histopathological changes and RGC loss in retinas without AOH modeling. However, after the KRT8 deficiency, AOH significantly promoted the loss of whole retina and inner retina thickness, the reduction, apoptosis, and dysfunction of RGCs, and the glial activation. Besides, downregulated Bcl-2 and upregulated cleaved-Caspase 3 were found in the AOH retinas with KRT8 knockdown, which may be caused by the increased phosphorylation level of MAPK pathways (JNK, p38, and ERK).

Conclusions. The KRT8 deficiency promoted RGC apoptosis and neurodegeneration by abnormal activation of MAPK pathways in AOH retinas. Targeting KRT8 may serve as a novel treatment for saving RCGs from glaucomatous injuries.

Keywords: keratin8, keratin18, retinal ganglion cell (RGC), glaucoma, acute ocular hypertension (AOH), MAPK pathway

Glaucoma, an optical neurodegenerative disease, is the leading cause of irreversible blindness worldwide.[1] The loss of retinal ganglion cells (RGCs) induced by pathologically high intraocular pressure (IOP) is the primary characteristic of glaucoma, except for some special types like normal tension glaucoma.[1,2] Considerable work has been done on the mechanisms of RGC damage under high IOP, including glutamate excitotoxicity, axonal transport failure, autophagy, endoplasmic reticulum stress, and oxidative stress.[3–8] Thus, the complicated molecular basis of RGC death or survival in response to this mechanical pressure stimulus has not been fully elucidated.[9]

Keratin (KRT) is an important member of the intermediate filament family, which helps form a complete network of cytoskeletal structures.[10] Keratin intermediate filaments require a type I (KRT9-28 and KRT31-40) and a type II keratin (KRT1-8 and KRT71-86) to form obligate heterodimers because the single type is unstable and easily degraded.[11] The specific pairings of keratins are expressed in tissue-, cellular-, differentiation-, and developmentally dependent manners.[12] KRT8 and KRT18 are the major paired keratins in simple epithelia, such as the liver, intestines, and pancreas.[13] In addition to providing mechanical stress resistance, previous studies have demonstrated that KRT8 exerts vital nonmechanical functions in the regulation of many physiological activities, such as cell proliferation, differentiation, apoptosis, autophagy, endoplasmic reticulum (ER) stress, and signal transduction.[14–20] However, few studies have focused on the expression and role of KRT8/18 in neurocytes, especially RGCs in the retina. There is also a vacancy in whether KRT8/18 responds to the stress of ocular hypertension and regulates the survival and death of RGCs via nonmechanical functions.

In this study, we identified the existence of KRT8/18 in the retinas and especially in RGCs, and the protein levels of KRT8/18 were increased by acute ocular hypertension (AOH) induction in mouse retinas. Our work demonstrated that AAV-mediated KRT8 knockdown in RGCs promoted the

RGC loss and dysfunction, and glial activation caused by ocular hypertension in a process where the abnormal activation of mitogen-activated protein kinase (MAPK) pathways may underlie the mechanism of aggravated RGC apoptosis.

Materials and Methods

Human Eye Tissue

The normal tissue of the human retina was obtained from a deceased healthy donor at the Department of Ophthalmology, the Second Affiliated Hospital, Medical College of Zhejiang University. Acquisitions and experiments involving human tissue were conducted in accordance with The Code of Ethics of the World Medical Association (Declaration of Helsinki) and were approved by the Human Research Ethics Committee of the Second Affiliated Hospital, Medical College of Zhejiang University (No. 120211118).

Animals Use and Statement

Male C57BL/6 mice were purchased from the Charles River Laboratories (Beijing, China) and housed in a temperature-controlled and pathogen-free facility with free access to clean water and food. All animal care and experiments were approved by the Laboratory Animal Ethics Committee of the Second Affiliated Hospital, Medical College of Zhejiang University (No. 2022-195) and performed in accordance with the Association for Research in Vision and Ophthalmology Statement for the Use of Animals in Ophthalmic and Vision Research.

AOH Model Induction

The procedure of AOH model induction was similar to our previous study.[21] After general and local anesthetized, mice (6-8 weeks old) were pupillary dilated by 0.5% tropicamide phenylephrine eye drops (Santen, Japan). A 33-gauge sterile needle was cannulated into the anterior chamber and attached to a saline reservoir with a height of 150 cm, realizing acute elevation of IOP to 110 mm Hg for 60 minutes. Then, the needle was removed to allow natural retinal reperfusion and the 0.5% levofloxacin antibiotic eye drop (Santen, Japan) was applied topically. Eyes with endophthalmitis, intraocular bleeding, cannulation-induced cataracts, or anterior chamber leakage were excluded.

AAV2-Mediated Downregulation of KRT8

The AAV2-hSyn-EGFP-KRT8-shRNA contained a hSyn neuron-specific promoter to induce the knockdown of KRT8 in RGCs and was purchased from Genechem Co., Ltd. (Shanghai, China) as well as the AAV2-hSyn-EGFP-control-shRNA. The 33-gauge Hamilton microsyringes (Hamilton Company, Reno, NV, USA) were used for intravitreal injection. Under anesthesia and pupillary dilation, mice (5 weeks old) were intravitreally injected with 1.5 µL (3.85×10^{12} v.g./mL) specific AAV2 and divided into two groups named the shCtrl group and the shKRT8 group. Three weeks after intravitreal injection, mice underwent anterior chamber perfusion to induce AOH injury.

Primary RGC Culture

The retina isolated from postnatal day 5 mice were dissected by microscopes and then dissociated with the papain (16.5 unit/mL) for acquiring single-cell suspensions. For RGC purification, the suspension was processed through 3-step panning: (i) incubation in a negative panning plate coated by the lectin for 30 min (shaken every 15 minutes); (ii) incubation in another lectin-coated dish for 10 minutes; and (iii) incubation in a positive panning plate coated by anti-mouse-Thy1.2 antibody (Bio-Rad Laboratories, Hercules, CA, USA) for 45 minutes (shaken every 15 minutes).[21,22] Then, cells attached to the plate were digested and collected for seeding on glass coverslips coated with mouse Laminin (R&D Systems, Minneapolis, MN, USA) and Poly-D Lysine (Sigma-Aldrich, St. Louis, MO, USA), and we cultured RGCs by the neurobasal medium containing supplemental factors in a humidified incubator containing 5% CO_2 and 95% air at 37°C.[21]

Hematoxylin and Eosin Staining Analysis

The eyeballs were fixed by Eyeball fixative solution (Haoke, Hangzhou, China) and embedded in paraffin. Then, 5-µm sections across the optic nerve were performed hematoxylin and eosin (H&E) staining and evaluated through light microscopy. The standard areas (300×300 µm^2, approximately 1 mm away from the optic disc) were chosen for measuring the thickness of the whole retina and sublayers of the retina, including the nerve fiber layer (NFL), the ganglion cell layer (GCL), the inner plexiform layer (IPL), the ganglion cell complex (GCC; which is composed of the NFL, the GCL, and the IPL), the inner nuclear layer (INL), the outer plexiform layer (OPL), and the outer nuclear layer (ONL) by Image-Pro Plus 6.0 (MediaCybernetics, Silver Spring, MD, USA).

Immunofluorescence

After dewaxing and antigen repair, retinal paraffin sections were blocked with the buffer (phosphate buffer saline [PBS] containing 5% goat serum, 0.5% BSA, and 0.05% Triton X-100) at room temperature (RT) for 1 hour. Then, the sections were incubated with primary antibodies (see Supplementary Table S1) at 4°C overnight and with species-specific secondary fluorescent antibodies (see Supplementary Table S1) at RT for 1 hour. DAPI was used for restaining before applying coverslips. The fluorescent images were captured by a Leica DMi8 microscope (Leica Microsystems, Panama). For RGC immunofluorescence, RGCs were fixed in 4% paraformaldehyde (PFA) at RT for 15 minutes and permeabilized in PBS with 0.5% Triton X-100 at RT for 15 minutes. The buffer (PBS with 10% goat serum and 0.1% Tween 20) was used for blocking. The remaining steps were the same as stated above.

For retinal flat-mounts immunofluorescence, after the eyes were fixed in 4% PFA for 1 hour at RT, the retinas were dissected and blocked in PBS containing 5% goat serum, 0.5% BSA, and 0.5% Triton X-100 for 1 hour at RT. Then, retinal tissues were incubated with the Brn3a antibody at 4°C overnight and with the secondary fluorescent antibody at RT for 3 hours. Next, the retinas were divided into four leaves and mounted with microscope slides. The fluorescent images were taken of the middle and peripheral areas of the retinal flat-mounts, which were approximately 1000 µm and 1700 µm, respectively, away from the optic disc.

Investigative Ophthalmology & Visual Science

In addition, the Brn3a-positive cells in a 300 × 300 μm^2 field were counted using ImageJ software (National Institutes of Health, Bethesda, MD, USA).

Immunohistochemistry

Dewaxed and antigen-repaired retinal paraffin sections were processed by Endogenous Peroxidase Blocking Solution (BOSTER, China) in the dark at RT for 10 minutes and blocked by goat serum at RT for 2 hours. The sections were incubated with primary antibodies (see Supplementary Table S1) at 37°C for 2 hours and with species-specific secondary antibodies (see Supplementary Table S1) at RT for 25 minutes, followed by staining with DAB Staining Kit (ZSGB-BIO, China). After redyeing with hematoxylin and dehydration with graded alcohol, we applied coverslips to the sections with neutral resin and observed them by a light microscope.

TUNEL Assay

Dewaxed retinal paraffin sections were processed by 20 μg/mL Proteinase K (Beyotime, China) at 37°C for 30 minutes. One Step TUNEL Apoptosis Assay Kit (Beyotime, China) was applied according to the instructions. The sections were incubated with TUNEL test solution at 37°C for 1 hour and then stained with DAPI. The number of both TUNEL and DAPI positive cells in the RGCLs was quantitated under the Leica DMi8 fluorescent microscope.

Transmission Electron Microscope

Separated retinas and optic nerves were fixed in precooled 2.5% glutaraldehyde at 4°C for 24 hours. The fixed retinas were merged in 1% OsO_4 for 1 hour and washed, followed by the dehydration and spurr embedding, as described previously.[21] Then 50-nm ultrathin sections, acquired via microtome (UC7; Leica Microsystems, Panama), were stained with uranyl acetate and lead citrate and examined under a transmission electron microscope (TEM; Tecnai G2 Spirit, FEI, Hillsboro, OR, USA).

Western Blot Analysis

Mouse retinas were isolated after eyeball enucleation and retinal pigment epithelium (RPE) layers were cleared as thoroughly as possible. Retina proteins were extracted from tissues by Protein Extraction Kit (Solarbio, China). Quantified protein samples were subjected to FuturePAGE Gels (ACE Biotechnology, China) for electrophoresis and transferred to PVDF membranes (Millipore, Temecula, CA, USA). After 1 hour blocking at RT by Protein Free Rapid Blocking Buffer (YaMei, China), membranes were incubated with primary antibodies (see Supplementary Table S1) at 4°C overnight and then with secondary antibodies (see Supplementary Table S1) at RT for 1 hour. The bands were detected by a Chemiluminescence imaging system (Bio-Rad, Hercules, CA, USA) and analyzed by ImageJ software. In the bands where each group contained two independent biological repeats, all samples from each group were computed and randomly matched before the electrophoresis, and the first sample in each group was normalized to the first one in the negative control group, and the second sample in each group was normalized to the second one in the negative control group.

Electroretinography

Mice were performed the full-field electroretinography (ERG) test under a Ganzfeld Q450C Stimulator (Roland, Germany). After anesthetization and pupillary dilation, recording electrodes were placed on the central cornea surface, and reference electrodes were placed hypodermically on the central forehead while grounding electrodes were inserted hypodermically into the tail. For evaluation of photopic negative response (PhNR), red light stimulation was performed at 0.4 cds/m^2 against a royal blue background of 25 cd/m^2 for 2 ms. The curve of PhNR was generated from the original data in GraphPad Prism 9.0 (GraphPad Software, Inc., San Diego, CA, USA), and the PhNR amplitude was referred to the electric potential from the baseline to a trough after the peak of the b wave.

Statistics

All experiments were performed at least three times in each group. The counts of independent biological replicates were shown by points in the statistical graphs and numbers in the figure legends. All data were presented as mean ± standard deviation (SD) unless indicated otherwise. The difference analysis was carried out by GraphPad Prism 9.0 using unpaired 2-tailed Student's *t*-test or 1-way analysis of variance (ANOVA) followed by Bonferroni post hoc test ($P < 0.05$ was considered statistically significant).

Results

The Expression of KRT8/18 in Retinas and Primary RGCs

We first examined the expression of KRT8/18 in the retinas of a normal human and mice by staining the tissue sections with KRT8/18 and Tuj-1 (a marker of RGCs). As shown in the immunofluorescent (IF) images (Fig. 1A), we found that KRT8/18 was expressed almost in the entire layer of the retina but was relatively more abundant in RGCs where KRT8/18 and Tuj-1 were colocalized. The results of immunohistochemistry staining also demonstrated that KRT8/18 was highly expressed in the GCL, which was more obvious in mouse retinas (Fig. 1B). Then, primary RGCs were purified and cultured from mice, and the expression of KRT8/18 was confirmed through double staining of Tuj-1 and KRT8/18 (Fig. 1C).

The Upregulation of KRT8/18 Expression by AOH

The expression pattern of KRT8/18 in retinas was investigated at 2 hours, 4 hours, 6 hours, 12 hours, 24 hours, and 72 hours using a mouse model of AOH.[23] Before protein extraction, RPE layers were cleared from collected retinas to avoid the influence of KRT8/18 in RPE layers.[24,25] As a whole, KRT8/18 expression increased gradually over time, peaked at approximately 12 hours, and then decreased, as shown by Western blot (WB) analysis (Figs. 1D, 1E). This signified that KRT8/18 may be involved in the regulation of RGC survival against AOH injuries.

AAV-Mediated KRT8 Knockdown in RGCs

For further study, we performed intravitreal injection of AAV2-hSyn-EGFP-KRT8-shRNA in C57BL/6 mice (5 weeks

Investigative Ophthalmology & Visual Science

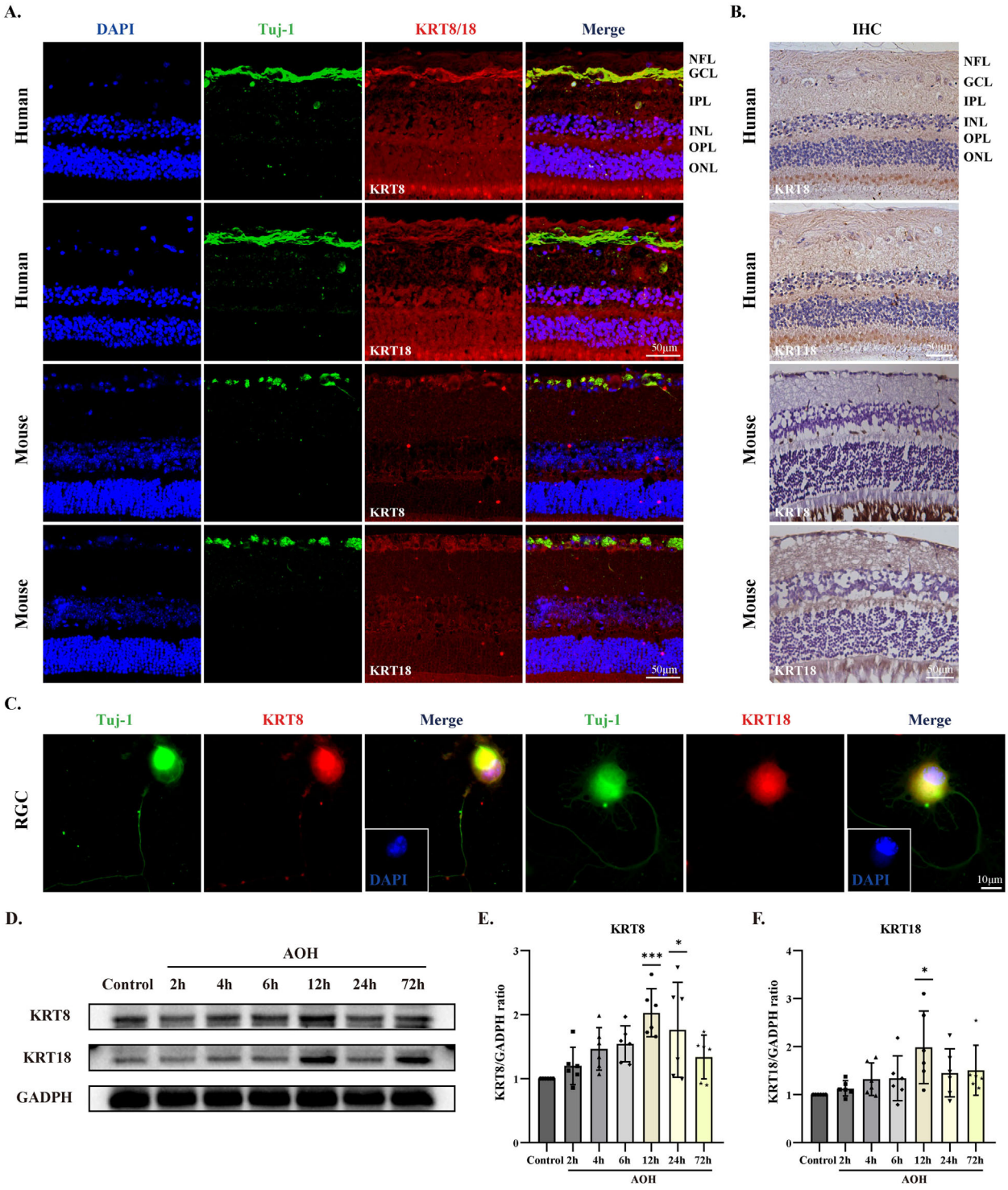

Figure 1. The expression of KRT8/18 in normal retinas and AOH retinas. (**A**) and (**C**) Representative immunofluorescence images of the normal human and mouse retinas (scale bar = 50 μm), and primary retinal ganglion cells (scale bar = 10 μm), labeled with DAPI (*blue*), Tuj-1 (*green*), and KRT8/18 (*red*). (**B**) Representative immunohistochemistry images of KRT8/18 in normal human and mouse retinas (scale bar = 50 μm). (**D**) Western blot bands of KRT8/18 in retinas at different times after the AOH treatment. (**E, F**) Quantitative analysis of the protein levels of KRT8 ($n = 6$) and KRT18 ($n = 6$), normalized to GADPH. Data were represented as mean ± SD, and analyzed using ANOVA; $^{*}P < 0.05$, $^{***}P < 0.01$ versus the control group.

old) for AAV-mediated KRT8 knockdown in RGCs. AAV2 contained the neuron-specific promoter Syn1, and its transduction was assessed 3 weeks after injection by co-staining retinal sections with GFP and Tuj-1, which showed that GFP was mainly colocalized with Tuj-1 (Supplementary Fig. S1). The expression level of KRT8/KRT18 in the retinas of the shKRT8 group was significantly downregulated to approximately 60% of the level in the shCtrl group, as shown

Investigative Ophthalmology & Visual Science

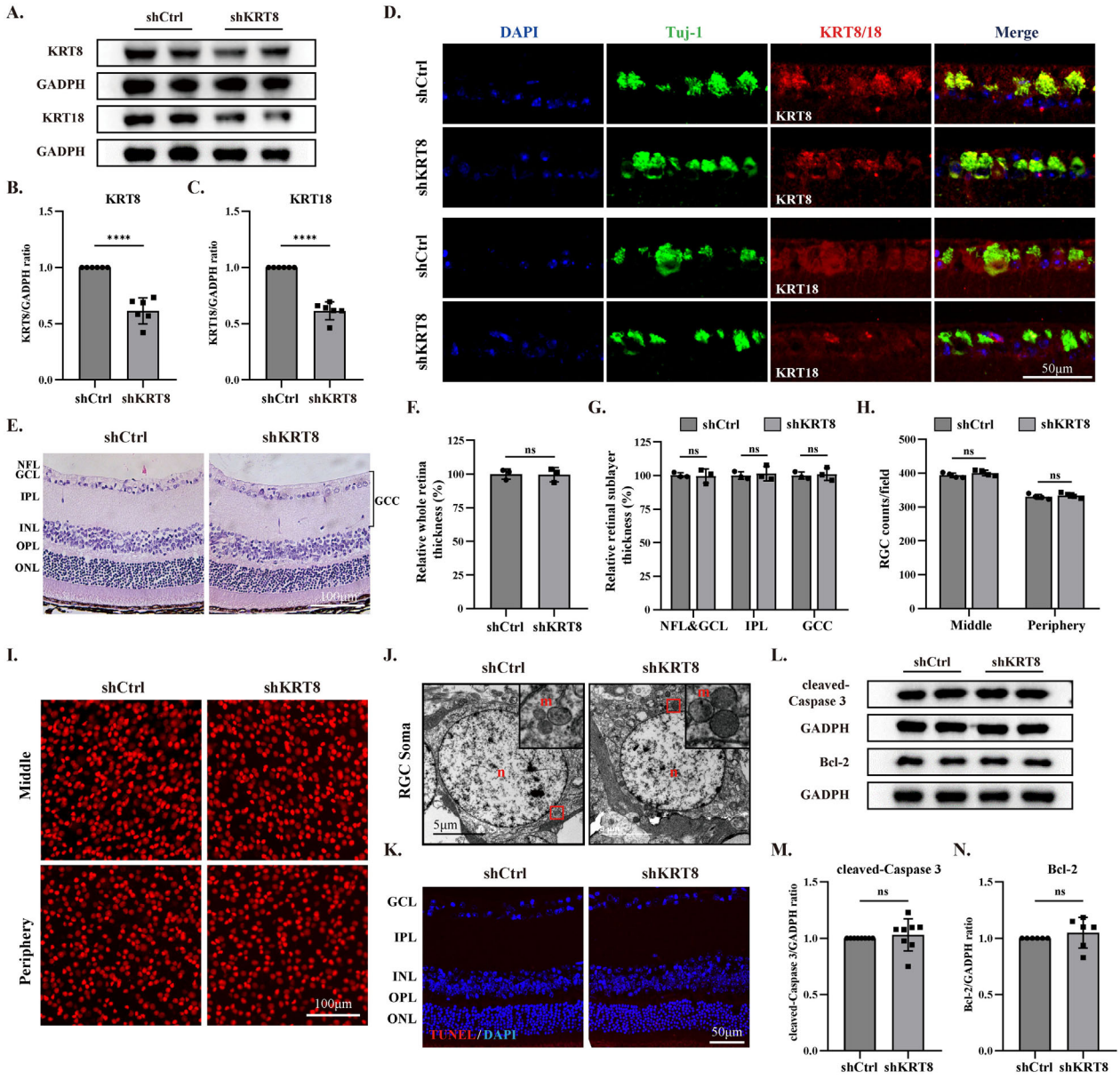

Figure 2. AAV-mediated reduction of KRT8 level in retinas. (**A**) and (**L**)Western blot bands of KRT8, KRT18, cleaved-Caspase 3, and Bcl-2 in retinas after AAV injection. (**B, C**) and (**M, N**) Quantitative analysis of the protein levels of KRT8, KRT18, cleaved-Caspase 3, and Bcl-2 normalized to GADPH ($n = 6$ or 8). (**D**) Representative immunofluorescence images of retinas after AAV injection, labeled with DAPI (*blue*), Tuj-1 (*green*), and KRT8/18 (*red*). Scale bar = 50 μm. (**E**) Representative H&E staining images of retinas after AAV injection. Scale bar = 100 μm. (**F, G**) Quantitative analysis of the thickness of the whole retina and retinal sublayers after AAV injection through H&E staining images ($n = 3$). (**H**) Quantitative analysis of the Brn3a-positive RGC counts in the middle and peripheral areas of retinal flat-mounts ($n = 4$). (**I**) Representative immunofluorescence images of retinal flat-mounts after AAV injection, labeled with Brn3a (red). Scale bar = 100 μm. (**J**) Ultrastructural observation of retinal RGCs after AAV injection via TEM (n = nuclei; m = mitochondria; and *red square* = the area of each inset). Scale bar = 5 μm. (**K**) Representative TUNEL staining images of retinas after AAV injection. Data were represented as mean ± SD, and analyzed using Student's *t*-test; $^{ns}P > 0.05$, $^{****}P < 0.0001$ versus the shCtrl group.

in the WB analysis (Figs. 2A–C). The weakened IF intensity of KRT8/18 in IF staining also illustrated the success of AAV-mediated KRT8 knockdown in RGCs (Fig. 2D). We also found no significant difference in the retinal structure, and the thickness of the whole retina and retinal sublayers, including the NFL & GCL, the IPL, the GCC, the INL, the OPL, and the ONL (Figs. 2E–G, Supplementary Fig. S2A). Moreover, we compared the RGC counts in the middle and periphery areas of the retinal flat-mounts stained with the Brn3a (a specific marker of RGCs). The results showed that the numbers of Brn3a-positive RGCs were not reduced after the KRT8 knockdown without AOH treatment (Figs. 2H–I). Regular cell nuclear and mitochondrial morphology could be observed in ultrastructural features of RGCs in both groups via TEM analysis (Fig. 2J). In addition, almost no TUNEL-positive cells were observed in either group of retinas (Fig. 2K). We also detected the expression of cleaved-Caspase 3 and Bcl-2 and found that there was no significant difference between the two groups (Figs. 2L–N). These results illustrated that AAV-mediated KRT8 knockdown did not cause histological or cytological abnormalities in the retina or the loss of RGCs under normal circumstances.

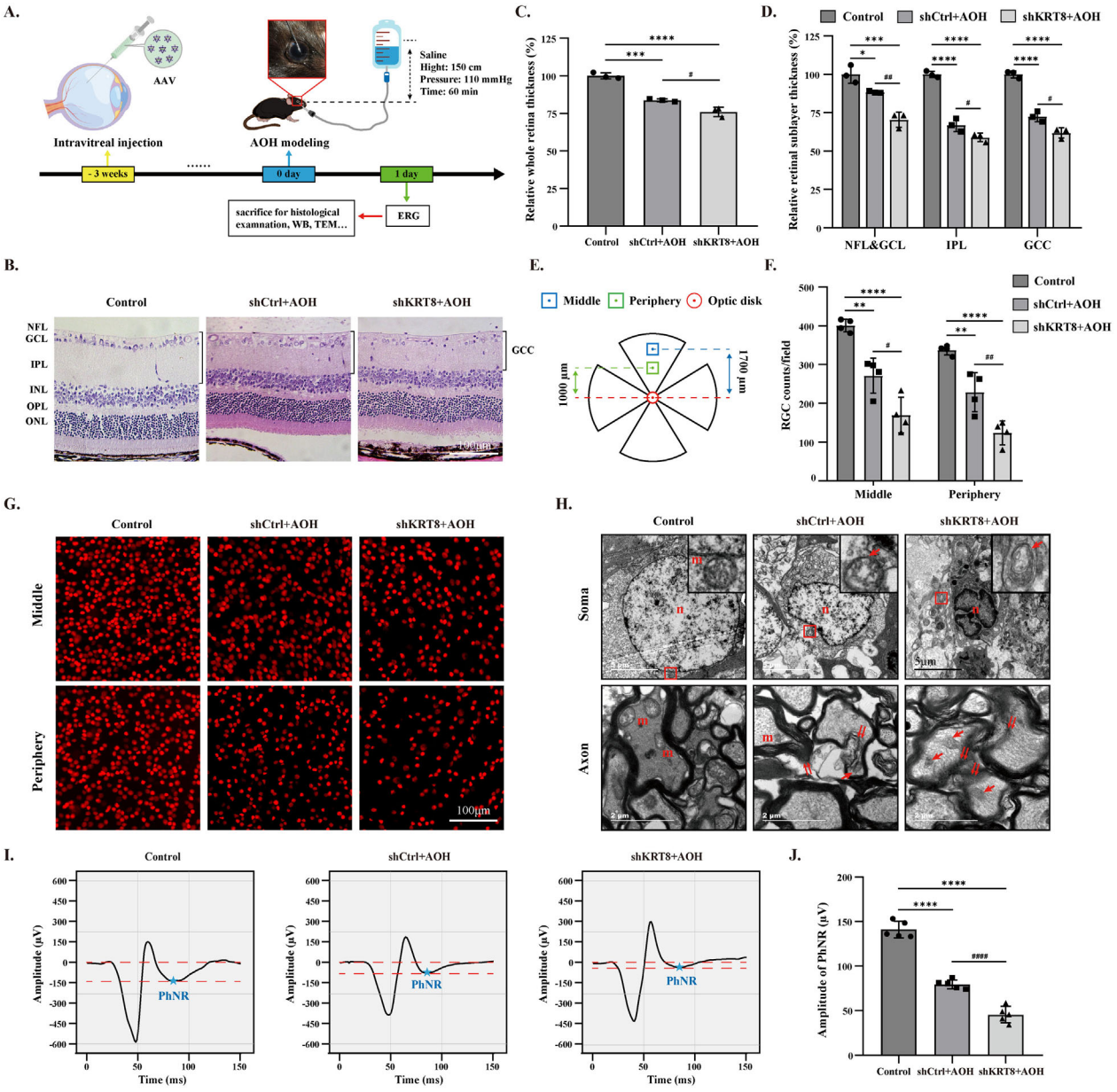

Figure 3. Keratin8 knockdown induced severer damage to RGCs in AOH retinas. (**A**) Schematic of the timeline and treatments of AAV intravitreal injection, AOH induction, and subsequent experiments. Note: Some used graphic materials are from the website of Figdraw. (**B**) Representative H&E staining images of retinas in different groups after AOH. Scale bar = 100 μm. (**C, D**) Quantitative analysis of the thickness of the whole retina and sublayers of the retinas after AAV injection through H&E staining images ($n = 3$). (**E**) Schematic of the middle and perpheiry areas of the retinal flat-mounts for the RGC counting. (**F**) Quantitative analysis of the Brn3a-positive RGC counts in the middle and peripheral areas of retinal flat-mounts ($n = 4$). (**G**) Representative immunofluorescence images of retinal flat-mounts in different groups after AOH, labeled with Brn3a (*red*). Scale bar = 100 μm. (**H**) Ultrastructural changes of RGC somas and axons in different groups after AOH. N = nuclei; m = mitochondria; *red arrow* = swollen or ruptured mitochondria; *double red arrow* = demyelination; *red square* = the area of each inset. Scale bar = 5 μm or 2 μm. (**I**) The representative curve of the PhNR of retinas in different groups after AOH. The pentagrams and the *dotted lines* marked the area between the baseline and the peak of PhNR. (**J**) Quantitative analysis of the PhNR amplitude in different groups after AOH ($n = 5$). Data were represented as mean ± SD, and analyzed using ANOVA; $^{*}P < 0.05$, $^{**}P < 0.001$, $^{***}P < 0.001$, $^{****}P < 0.0001$ versus the control group; $^{\#}P < 0.05$, $^{\#\#}P < 0.01$, $^{\#\#\#\#}P < 0.0001$ versus the shCtrl + AOH group.

Keratin8 Knockdown Led to More Severe Injuries in RGCs After AOH

To investigate the role of KRT8 in RGCs under glaucomatous injuries, mice were treated with anterior perfusion 3 weeks after AAV injection and applied to other experiments 24 hours after AOH induction (Fig. 3A). The elevation of KRT8 expression was reversed by AAV-mediated interference (Supplementary Fig. S3). Through H&E staining, AOH in the shKRT8 group was found to induce a more severe decrease in the thickness of the whole retina, the NFL & GCL, the IPL and the GCC, compared with the shCtrl group (see Figs. 3C, 3D, Supplementary Fig. S2B). Meanwhile, the immunofluorescence of retinal flat-mounts showed that the

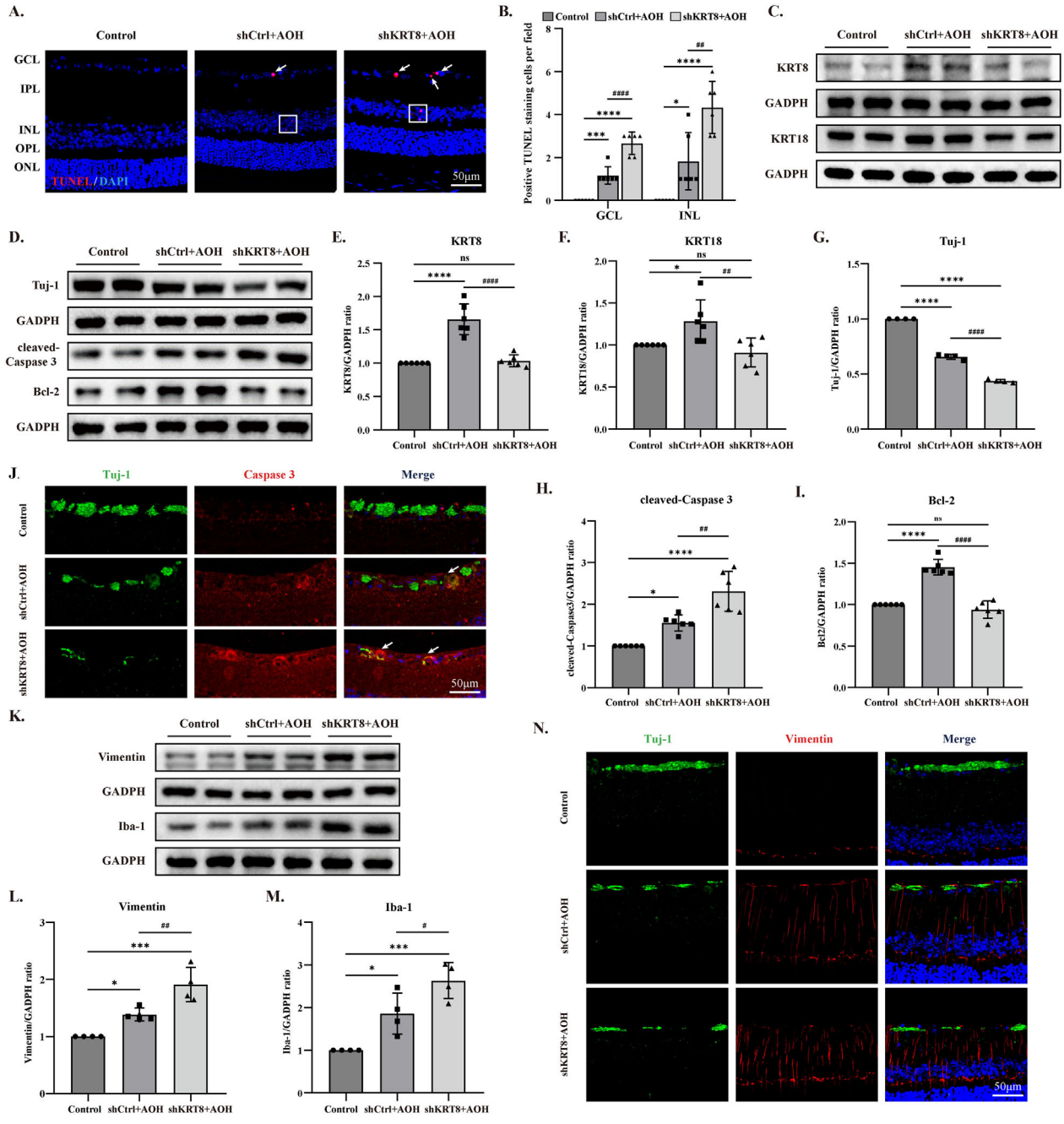

Figure 4. Keratin8 knockdown promoted RGC apoptosis and glial cell activation after AOH induction. (**A**) Representative TUNEL staining images in different groups after AOH. *White arrow* = cells with positive TUNEL staining in the GCL; and *white square* = cells with positive TUNEL staining in the INL. (**B**) Quantitative analysis of the cell number with positive TUNEL staining ($n = 6$). (**C, D**) and (**K**) Western blot bands of KRT8, KRT18, Tuj-1, cleaved-Caspase 3, Bcl-2, Vimentin, and Iba-1 of retinas in different groups after AOH. (**E-I**) and (**L, M**) Quantitative analysis of the protein levels of KRT8, KRT18, Tuj-1, cleaved-Caspase 3, Bcl-2, Vimentin, and Iba-1, normalized to GADPH ($n = 4$ or 6). (**J**) and (**N**) Representative immunofluorescence images of retinas, labeled with DAPI (*blue*), Tuj-1 (*green*), and Caspase 3, or Vimentin (Red). *White arrow* = typical RGCs with staining of Tuj-1 and Caspase 3. Scale bar = 50 μm. Data were represented as mean ± SD, and analyzed using ANOVA; $^{ns}P > 0.05$; $^{*}P < 0.05$, $^{***}P < 0.001$, $^{****}P < 0.0001$ versus the control group; $^{\#}P < 0.01$, $^{\#\#}P < 0.01$, $^{\#\#\#\#}P < 0.0001$ versus the shCtrl + AOH group.

RGCs counts were markedly decreased after AOH treatment, and the KRT8 deficiency caused more loss of RGCs in the shKRT8 + AOH group than the shCtrl + AOH group (Figs. 3E–G). Ultrastructural changes were also examined through TEM images (Fig. 3H). After AOH, the nuclei and mitochondria in RGC somas began to lose their normal shape and structure. However, the shKRT8 group showed more classical characteristics of cellular apoptosis, where the nucleus was shrunken and fragmented along with denser chromatin distributed against the nuclear envelope. In addition to soma formation, the demyelination and mitochondrial destruction of RGC axons were exacerbated. Next, we examined the

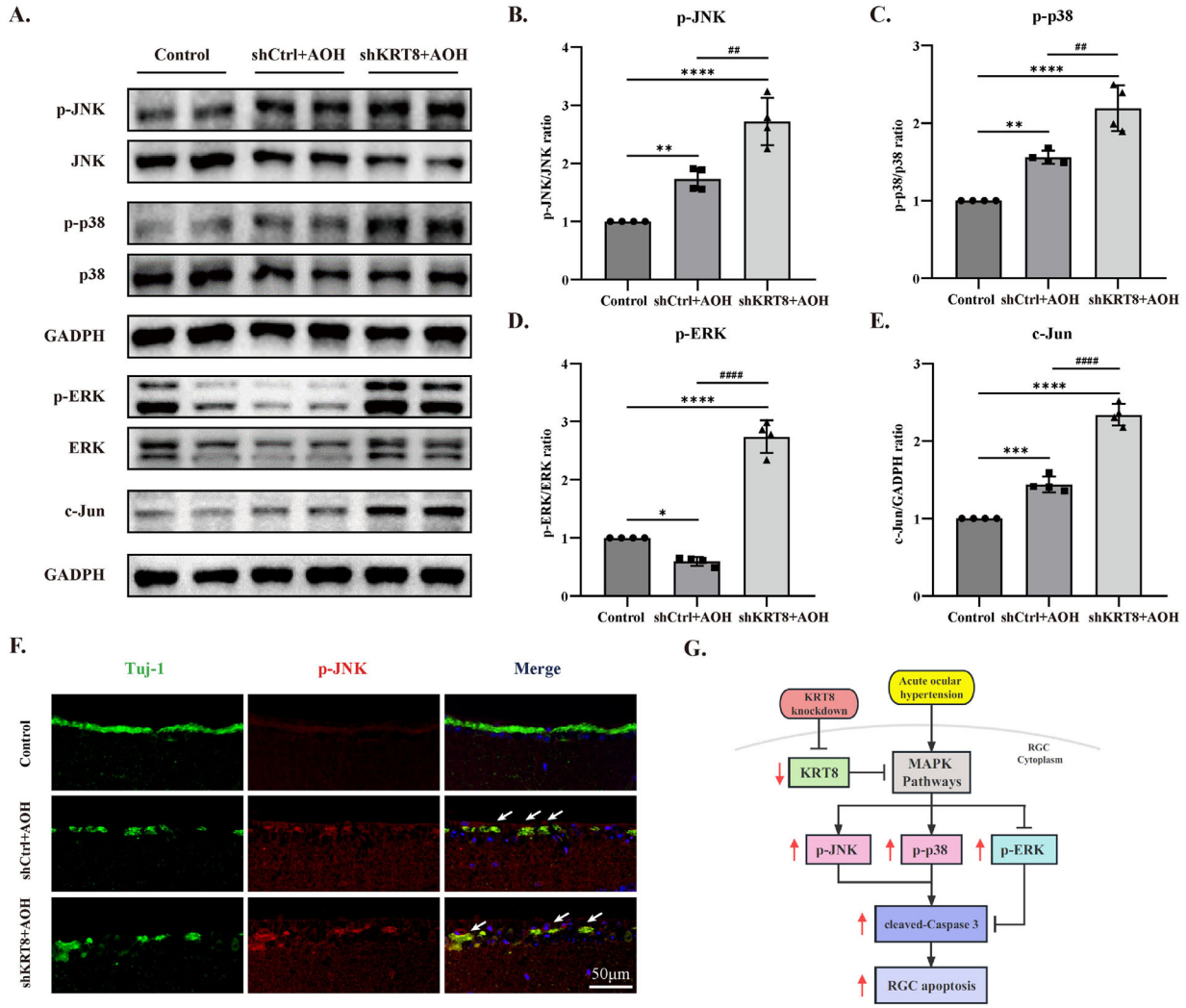

Figure 5. Keratin8 knockdown promoted the activation of MAPK pathways after AOH induction. (**A**) Western blot bands of p-JNK, JNK, p-p38, p38, p-ERK, ERK, and c-Jun of retinas in different groups after AOH. (**B-E**) Quantitative analysis of the protein levels of p-JNK, p38, p-ERK, and c-Jun, normalized to their unphosphorylated proteins or GADPH ($n = 4$). (**F**) Representative immunofluorescence images of retinas, labeled with DAPI (*blue*), Tuj-1 (*green*), and p-JNK (*red*). *White arrow* = typical RGCs with staining of Tuj-1 and p-JNK. Scale bar = 50 µm. (**G**) Schematic of the mechanism of KRT8 in the RGC apoptosis under AOH. The *red arrows* represent the final change under the condition of the KRT8 knockdown. Data were represented as mean ± SD, and analyzed using ANOVA; $^{*}P < 0.05$, $^{**}P < 0.01$, $^{***}P < 0.001$, $^{****}P < 0.0001$ versus the control group; $^{\#\#}P < 0.01$, $^{\#\#\#\#}P < 0.0001$ versus the shCtrl + AOH group.

severity of RGC function loss via the detection of the PhNR (representing the generalized activity of RGCs and their axons) of the light-adapted ERG.[26–28] The PhNR amplitude in the shKRT8 group (79.7 ± 4.97 µV) was significantly lower than that in the shCtrl group (45.6 ± 9.15 µV), as shown in Figures 3I–J. Besides, we found the amplitude of a-wave and b-wave had a wide range and no significant statistical difference were found among the three groups. These results indicated that AAV-mediated KRT8 knockdown in RGCs led to more severe injuries in RGCs after AOH, inducing worse visual function.

Keratin8 Knockdown Promoted RGC Apoptosis and Glial Cell Activation After AOH

Here, we focused on whether KRT8 knockdown contributed to RGC apoptosis in AOH retinas. TUNEL assays showed that there were almost few TUNEL-positive cells in control retinas, but the numbers of TUNEL-positive cells in the GCL and INL were increased after AOH, which was significantly greater in the shKRT8 group than in the shCtrl group (Figs. 4A, 4B). According to the results of WB, the AAV-mediated KRT8 knockdown caused lower expression levels of KRT8, KRT18, Tuj-1, and Bcl-2 but a higher expression level of cleaved-Caspase 3 in AOH retinas (Figs. 4C–I). Additionally, as indicated by the immunofluorescence results, the density of Caspase 3 in the GCL, especially in RGCs, was significantly upregulated (Fig. 4J). These results indicated that KRT8 knockdown seriously promoted the apoptosis of RGCs under AOH injury.

Interestingly, we also found more severe activation of glial cells in the retinas of the shKRT8 group with AOH, indicating the degree of neuroinflammation.[29,30] The expression of Vimentin (a marker of Müller cells) and Iba-1 (a marker of microglia), was significantly enhanced (Figs. 4K–

M), which was consistent with more obvious morphologic alterations and more numbers of glial cells observed in IF images stained with Vimentin or Iba-1 in the shKRT8 + AOH group (Fig. 4N, Supplementary Fig. S4).

MAPK Pathway Activation in RGCs With Keratin8 Knockdown After AOH

Then, we examined whether the reduction in KRT8 regulated the MAPK pathways, including c-Jun N-terminal kinase (JNK), p38 MAPK, and extracellular signal-regulated protein kinase (ERK). As shown in WB analysis, the expression of p-JNK, p-p38, and c-Jun (a downstream effector protein of MAPK pathways) was upregulated but not p-ERK in the retinas of the shCtrl + AOH group compared with the control group (Figs. 5A–E). However, the knockdown of KRT8 significantly induced more protein phosphorylation of p38, JNK, and ERK and more expression of c-Jun than in the shCtrl group with AOH (Figs. 5A–E). We also observed stronger IF signaling of p-JNK in RGCs of the shKRT8 group with AOH (Fig. 5F). Thus, abnormal MAPK pathway activation may underlie the mechanism of aggravated damage in RGCs with KRT8 knockdown under AOH.

Discussion

In this study, we verified the distribution of KRT8/18 in the retina and RGCs were the most abundantly expressed cells in retinas (except for the RPE), and we found their expressions increased in the mouse AOH model. Furthermore, by selectively knockdown of KRT8 in RGCs, we demonstrated the key role of KRT8 in RGC resistance to ocular hypertension in a process involved in the activation of MAPK pathways. The findings provide new insights and directions into the mechanisms of RGC damage in glaucoma.

Keratins are well-known markers of epithelial cells and have a cell-specific expression pattern that distinguishes different epithelial cell types.[10–12] Interestingly, KRT8 was found to be present in olfactory neurons and other classes of olfactory epithelial cells, although the presence of keratins was once thought unusual in normal developing or mature neurons of mammals.[31–33] Here, we considered that the existence of KRT8/18 in retinas and the relatively high abundance in RGCs may be correlated with the origin of retinas in that the inner layer of the optic cup produces the retinal neuroepithelium layer, whereas the outer layer forms the RPE layer.[34]

The preservation of KRT8/18 in RCGs through the developmental process may be meaningful for responding to intraocular mechanical stresses, such as the pathological IOP elevation in glaucoma. The AOH model, also known as the retinal ischemia-reperfusion (IR) model, is a widely used and ideal model to simulate the pathogenesis of acute primary angle-closure glaucoma which leads to the IR injury and then RGC loss after sudden and acute IOP elevation.[21,23,35,36] Through our examination after AOH induction, the expression of KRT8 was first upregulated and peaked at approximately 12 hours or 24 hours, and our previous study found that TUNEL-positive staining of RGCs began to be observed at 24 hours, which seemed to be in parallel with the downregulation of KRT8/18.[21] Indeed, the remodeling and degradation of cytoskeleton proteins are involved in the apoptosis process, and type I keratins including KRT18, not type II, serve as the major caspase substrates, whose caspase-generated fragments are used as biomarkers for cancer and liver injury.[11,13,37]

AAV is commonly used to deliver transgenes to RGCs.[36,38–41] Nieuwenhuis et al. compared the gene delivery of AAV2 with five promoters, and they found the strongest expression of EGFP in the retina driven by hSyn promoters, as well as almost exclusive transgene expression in RGCs.[42] We also generated neuron-specific knockdown of KRT8 in mouse retinas via intravitreal injection of AAV2 with the hSyn promoter.[39,43] Under normal conditions, the knockdown of KRT8 did not induce RGC apoptosis and ultrastructural changes, which indicated that KRT8 is not indispensable to nonstressful RGCs.

However, this study further found that apoptotic changes were significantly aggravated by KRT8 downregulation in RGCs after AOH treatment, resulting in a more serious decrease in visual function assessed by PhNR in ERG. On the other hand, more severe activation of Müller cells and microglia reflected the elevated level of apoptotic RGCs to some extent, which promoted retinal neuroinflammation. It has been demonstrated that keratins can be involved in the regulation of apoptosis through several mechanisms.[44] For example, KRT8 and KRT18 allow simple epithelial cells to resist TNF-induced death by binding the cytoplasmic domain of TNFR2.[45] It is worth noting that KRT8 is a substrate of various stress-activated protein kinases (SAPKs), including JNK, p38, and ERK, and the deletion of KRT8 or the inhibition of KRT8 phosphorylation sites can result in the dysregulated activation of other substrates (such as c-Jun) of SAPKs.[14,20,46–48]

In fact, the SAPKs of JNK, p38 MAPK, and ERK belong to the MAPK family of serine/threonine protein kinases, which can transduce environmental stress signals into regulated gene expression.[49] Abundant studies have shown that MAPK pathways play essential roles in the pathogenesis of glaucomatous RGC apoptosis.[3,9,50,51] It is generally accepted that the activation of JNK and p38 via phosphorylation is a proapoptotic signal. The administration of inhibitors blocking JNK or p38 activity can protect against RGC death induced by acute or chronic ocular hypertension.[52–56] c-Jun was expressed in a pattern parallel with glaucomatous injury, whereas its deficiency protected RGC somas from ocular hypertensive injury.[57] In contrast, ERK1/2 activation is generally neuroprotective in glaucoma and other neurodegenerative diseases.[3,50,58,59] The level of p-ERK1/2 was found to be downregulated in ocular hypertension conditions.[43] Our results also found a significant increase in p-JNK and p-p38 levels and a decrease in p-ERK levels, which accounted for RGC apoptosis in the shCtrl + AOH group. However, under high IOP conditions, AAV-mediated KRT8 knockdown significantly exacerbated RGC injuries by increasing the phosphorylation levels of JNK and p38 and upregulating the expression level of c-Jun compared to those in the shCtrl + AOH group. The downregulation of p-ERK by high IOP was also reversed by KRT8 knockdown, which was contradictory to the final outcoming of aggravated apoptosis or more loss of RGCs. The explanation may be that the proapoptotic effect of KRT8 deficiency is likely to be multifactorial and may also involve increasing Fas receptors on the cell surface, as noted in KRT8-null hepatocytes, and promoting TNF-induced death.[17,45] Besides, the over-elevation of p-ERK can result in the activation of the NF-κB signaling pathway, and its blockage alleviates the inflammatory response, including gliosis.[60–62] Thus, the severer activated and proliferated Müller cells and microglia in the shKRT8 + AOH

Investigative Ophthalmology & Visual Science

group may contribute to the increased p-ERK level in whole retinas, which underlies the mechanism of the neuroprotection effect of the ERK inhibitor under ocular hypertensive injury or axotomy of the optic nerve.[63–66] Here, we hypothesized that KRT8 may at least serve as a sponge of activated SAPKs in RGCs and that the deletion of KRT8 can lead to the abnormal activation of MAPK pathways and then the downstream apoptotic cascade under AOH stress in glaucoma. However, the role of KRT8 is needed to be further verified in primary RGCs under pressure combined with the treatment of oxygen-glucose deprivation in vitro, and whether other regulatory mechanisms are involved in the neuroprotective function of KRT should be investigated in the future.

In summary, this study provided the first evidence of the existence of KRT8/18 in RGCs. Our results demonstrated that the KRT8 reduction leads to excessive phosphorylated JNK, p38, and ERK of MAPK pathways and thereby induces downstream proapoptotic events to promote RGC death under glaucomatous stress in ocular hypertension (Fig. 5G). Therefore, we suggest that KRT8 is a novel neuroprotective target in glaucoma and warrants further investigation into deeper regulatory mechanisms.

Acknowledgments

The authors thank Beibei Wang in the Center of Cryo-Electron Microscopy, Zhejiang University for her technical assistance with TEM.

Supported by the National Natural Science Foundation of China (No. 82171045) and the Key Program of the National Natural Science Foundation of Zhejiang Province (No. LZ23H120001).

Authors' Contributions: M.C. and K.W. designed the study and revised the manuscript. C.Z., N.Y., and Q.Q. performed the experiments and conducted the writing and review of the article. X.W., Y.G., and T.L. provided acquisition, analysis, and interpretation of the data. Q.Z. and X.L. provided technical and material support. All authors read and approved the final paper.

Disclosure: **C. Zhang**, None; **N. Yu**, None; **Q. Qin**, None; **X. Wu**, None; **Y. Gu**, None; **T. Liu**, None; **Q. Zhang**, None; **X. Liu**, None; **M. Chen**, None; **K. Wang**, None

References

1. Quigley HA. Glaucoma. *Lancet*. 2011;377(9774):1367–1377.
2. Wu X, Konieczka K, Liu X, et al. Role of ocular blood flow in normal tension glaucoma. *Adv Ophthalmol Pract Res*. 2022;2(1):100036.
3. Almasieh M, Wilson AM, Morquette B, Cueva Vargas JL, Di Polo A. The molecular basis of retinal ganglion cell death in glaucoma. *Prog Retin Eye Res*. 2012;31(2):152–181.
4. Hartwick ATE, Hamilton CM, Baldridge WH. Glutamatergic calcium dynamics and deregulation of rat retinal ganglion cells. *J Physiol*. 2008;586(14):3425–3446.
5. Seki M, Lipton SA. Targeting excitotoxic/free radical signaling pathways for therapeutic intervention in glaucoma. *Prog Brain Res*. 2008;173:495–510.
6. Salinas-Navarro M, Alarcón-Martínez L, Valiente-Soriano FJ, et al. Ocular hypertension impairs optic nerve axonal transport leading to progressive retinal ganglion cell degeneration. *Exp Eye Res*. 2010;90(1):168–183.
7. Izzotti A, Bagnis A, Saccà SC. The role of oxidative stress in glaucoma. *Mutat Res*. 2006;612(2):105–114.
8. Russo R, Nucci C, Corasaniti MT, Bagetta G, Morrone LA. Chapter 4 - Autophagy dysregulation and the fate of retinal ganglion cells in glaucomatous optic neuropathy. In: Bagetta G, Nucci C, eds. *Progress in Brain Research. Vol. 220. New Trends in Basic and Clinical Research of Glaucoma: A Neurodegenerative Disease of the Visual System, Part A*. New York, NY: Elsevier; 2015:87–105.
9. Völgyi B. Molecular biology of retinal ganglion cells. *Cells*. 2020;9(11):2483.
10. Coulombe PA, Omary MB. 'Hard' and 'soft' principles defining the structure, function and regulation of keratin intermediate filaments. *Curr Opin Cell Biol*. 2002;14(1):110–122.
11. Jacob JT, Coulombe PA, Kwan R, Omary MB. Types I and II keratin intermediate filaments. *Cold Spring Harb Perspect Biol*. 2018;10(4):a018275.
12. Szeverenyi I, Cassidy AJ, Chung CW, et al. The Human Intermediate Filament Database: comprehensive information on a gene family involved in many human diseases. *Hum Mutat*. 2008;29(3):351–360.
13. Loschke F, Seltmann K, Bouameur JE, Magin TM. Regulation of keratin network organization. *Curr Opin Cell Biol*. 2015;32:56–64.
14. Ku NO, Omary MB. A disease- and phosphorylation-related nonmechanical function for keratin 8. *J Cell Biol*. 2006;174(1):115–125.
15. Miao Q, Xu Y, Yin H, Zhang H, Ye J. KRT8 phosphorylation regulates the epithelial-mesenchymal transition in retinal pigment epithelial cells through autophagy modulation. *J Cell Mol Med*. 2020;24(5):3217–3228.
16. Lähdeniemi IAK, Misiorek JO, Antila CJM, et al. Keratins regulate colonic epithelial cell differentiation through the Notch1 signalling pathway. *Cell Death Differ*. 2017;24(6):984–996.
17. Gilbert S, Loranger A, Daigle N, Marceau N. Simple epithelium keratins 8 and 18 provide resistance to Fas-mediated apoptosis. The protection occurs through a receptor-targeting modulation. *J Cell Biol*. 2001;154(4):763–774.
18. Baek A, Yoon S, Kim J, et al. Autophagy and KRT8/keratin 8 protect degeneration of retinal pigment epithelium under oxidative stress. *Autophagy*. 2017;13(2):248–263.
19. Wang D, Zhang P, Xu X, et al. Knockdown of cytokeratin 8 overcomes chemoresistance of chordoma cells by aggravating endoplasmic reticulum stress through PERK/eIF2α arm of unfolded protein response and blocking autophagy. *Cell Death Dis*. 2019;10(12):887.
20. Guldiken N, Zhou Q, Kucukoglu O, et al. Human keratin 8 variants promote mouse acetaminophen hepatotoxicity coupled with JNK activation and protein adduct formation. *Hepatology*. 2015;62(3):876–886.
21. Qin Q, Yu N, Gu Y, et al. Inhibiting multiple forms of cell death optimizes ganglion cells survival after retinal ischemia reperfusion injury. *Cell Death Dis*. 2022;13(5):507.
22. Winzeler A, Wang JT. Purification and culture of retinal ganglion cells from rodents. *Cold Spring Harb Protoc*. 2013;2013(7):643–652.
23. Hartsock MJ, Cho H, Wu L, Chen WJ, Gong J, Duh EJ. A mouse model of retinal ischemia-reperfusion injury through elevation of intraocular pressure. *J Vis Exp*. 2016;(113):54065.
24. Hunt RC, Davis AA. Altered expression of keratin and vimentin in human retinal pigment epithelial cells in vivo and in vitro. *J Cell Physiol*. 1990;145(2):187–199.
25. Vossmerbaeumer U, Ohnesorge S, Kuehl S, et al. Retinal pigment epithelial phenotype induced in human adipose tissue-derived mesenchymal stromal cells. *Cytotherapy*. 2009;11(2):177–188.
26. Frishman L, Sustar M, Kremers J, et al. ISCEV extended protocol for the photopic negative response (PhNR)

Investigative Ophthalmology & Visual Science

of the full-field electroretinogram. *Doc Ophthalmol*. 2018;136(3):207–211.
27. Viswanathan S, Frishman LJ, Robson JG, Harwerth RS, Smith EL. The photopic negative response of the macaque electroretinogram: reduction by experimental glaucoma. *Invest Ophthalmol Vis Sci*. 1999;40(6):1124–1136.
28. Colotto A, Falsini B, Salgarello T, Iarossi G, Galan ME, Scullica L. Photopic negative response of the human ERG: losses associated with glaucomatous damage. *Invest Ophthalmol Vis Sci*. 2000;41(8):2205–2211.
29. Hu X, Zhao GL, Xu MX, et al. Interplay between Müller cells and microglia aggravates retinal inflammatory response in experimental glaucoma. *J Neuroinflammation*. 2021;18:303.
30. Tezel G. Molecular regulation of neuroinflammation in glaucoma: current knowledge and the ongoing search for new treatment targets. *Prog Retin Eye Res*. 2022;87:100998.
31. Trojanowski JQ, Newman PD, Hill WD, Lee VM. Human olfactory epithelium in normal aging, Alzheimer's disease, and other neurodegenerative disorders. *J Comp Neurol*. 1991;310(3):365–376.
32. Ophir D. Intermediate filament expression in human fetal olfactory epithelium. *Arch Otolaryngol Head Neck Surg*. 1987;113(2):155–159.
33. Franko MC, Gibbs CJ, Rhoades DA, Gajdusek DC. Monoclonal antibody analysis of keratin expression in the central nervous system. *Proc Natl Acad Sci U S A*. 1987;84(10):3482–3485.
34. Graw J. Eye Development. In: *Current Topics in Developmental Biology*. Vol. 90. New York, NY: Elsevier; 2010:343–386.
35. Ye D, Xu Y, Shi Y, et al. Anti-PANoptosis is involved in neuroprotective effects of melatonin in acute ocular hypertension model. *J Pineal Res*. 2022;73(4):e12828.
36. Liu W, Ha Y, Xia F, et al. Neuronal Epac1 mediates retinal neurodegeneration in mouse models of ocular hypertension. *J Exp Med*. 2020;217(4):e20190930.
37. Monier B, Suzanne M. Orchestration of force generation and nuclear collapse in apoptotic cells. *Int J Mol Sci*. 2021;22(19):10257.
38. Ha Y, Liu W, Liu H, et al. AAV2-mediated GRP78 transfer alleviates retinal neuronal injury by downregulating ER stress and tau oligomer formation. *Invest Ophthalmol Vis Sci*. 2018;59(11):4670–4682.
39. Guo X, Zhou J, Starr C, et al. Preservation of vision after CaMKII-mediated protection of retinal ganglion cells. *Cell*. 2021;184(16):4299–4314.e12.
40. Tan J, Zhang X, Li D, et al. scAAV2-mediated C3 transferase gene therapy in a rat model with retinal ischemia/reperfusion injuries. *Molec Ther Meth Clinic Devel*. 2020;17:894.
41. Wang Q, Zhuang P, Huang H, et al. Mouse γ-synuclein promoter-mediated gene expression and editing in mammalian retinal ganglion cells. *J Neurosci*. 2020;40(20):3896–3914.
42. Nieuwenhuis B, Laperrousaz E, Tribble JR, et al. Improving adeno-associated viral (AAV) vector-mediated transgene expression in retinal ganglion cells: comparison of five promoters. *Gene Ther*. 2023;30(6):503–519.
43. Basavarajappa D, Gupta V, Wall RV, et al. S1PR1 signaling attenuates apoptosis of retinal ganglion cells via modulation of cJun/Bim cascade and Bad phosphorylation in a mouse model of glaucoma. *FASEB J*. 2023;37(1):e22710.
44. Arin MJ. The molecular basis of human keratin disorders. *Hum Genet*. 2009;125(4):355–373.
45. Caulin C, Ware CF, Magin TM, Oshima RG. Keratin-dependent, epithelial resistance to tumor necrosis factor-induced apoptosis. *J Cell Biol*. 2000;149(1):17–22.
46. He T, Stepulak A, Holmström TH, Omary MB, Eriksson JE. The intermediate filament protein keratin 8 is a novel cytoplasmic substrate for c-Jun N-terminal kinase*. *J Biol Chem*. 2002;277(13):10767–10774.
47. Ku NO, Omary MB, Azhar S. Keratin 8 Phosphorylation by p38 kinase regulates cellular keratin filament reorganization: modulation by a keratin 1-like disease-causing mutation*. *J Biol Chem*. 2002;277(13):10775–10782.
48. Lim Y, Ku NO. Revealing the roles of keratin 8/18-associated signaling proteins involved in the development of hepatocellular carcinoma. *Int J Mol Sci*. 2021;22(12):6401.
49. Chang L, Karin M. Mammalian MAP kinase signalling cascades. *Nature*. 2001;410(6824):37–40.
50. Levkovitch-Verbin H. Chapter 2 - Retinal ganglion cell apoptotic pathway in glaucoma: initiating and downstream mechanisms. In: Bagetta G, Nucci C, eds. *Progress in Brain Research*. Vol 220. *New Trends in Basic and Clinical Research of Glaucoma: A Neurodegenerative Disease of the Visual System, Part A*. New York, NY: Elsevier; 2015:37–57.
51. Yuan J, Yankner BA. Apoptosis in the nervous system. *Nature*. 2000;407(6805):802–809.
52. Liu H, Sun H, Liu C. Interference of the apoptotic signaling pathway in RGC stress response by SP600125 in moderate ocular hypertensive rats. *Chin J Physiol*. 2011;54(2):124–132.
53. Sun H, Wang Y, Pang IH, et al. Protective effect of a JNK inhibitor against retinal ganglion cell loss induced by acute moderate ocular hypertension. *Mol Vis*. 2011;17:864–875.
54. Kim BJ, Silverman SM, Liu Y, Wordinger RJ, Pang IH, Clark AF. In vitro and in vivo neuroprotective effects of cJun N-terminal kinase inhibitors on retinal ganglion cells. *Molec Neurodegen*. 2016;11(1):30.
55. Dapper JD, Crish SD, Pang IH, Calkins DJ. Proximal inhibition of p38 MAPK stress signaling prevents distal axonopathy. *Neurobiol Dis*. 2013;59:26–37.
56. Lambert WS, Pasini S, Collyer JW, et al. Of mice and monkeys: neuroprotective efficacy of the p38 inhibitor BIRB 796 depends on model duration in experimental glaucoma. *Sci Rep*. 2020;10(1):8535.
57. Syc-Mazurek SB, Fernandes KA, Libby RT. JUN is important for ocular hypertension-induced retinal ganglion cell degeneration. *Cell Death Dis*. 2017;8(7):e2945.
58. Rai SN, Dilnashin H, Birla H, et al. The role of PI3K/Akt and ERK in neurodegenerative disorders. *Neurotox Res*. 2019;35(3):775–795.
59. Zhou Y, Pernet V, Hauswirth WW, Di Polo A. Activation of the extracellular signal-regulated kinase 1/2 pathway by AAV gene transfer protects retinal ganglion cells in glaucoma. *Molec Ther*. 2005;12(3):402–412.
60. Nakano H, Shindo M, Sakon S, et al. Differential regulation of IkappaB kinase alpha and beta by two upstream kinases, NF-kappaB-inducing kinase and mitogen-activated protein kinase/ERK kinase kinase-1. *Proc Natl Acad Sci USA*. 1998;95(7):3537–3542.
61. Syed Hussein SS, Kamarudin MNA, Kadir HA. (+)-Catechin attenuates NF-κB activation through regulation of Akt, MAPK, and AMPK signaling pathways in LPS-induced BV-2 microglial cells. *Am J Chin Med*. 2015;43(5):927–952.
62. Jiang T, Gong Y, Zhang W, et al. PD0325901, an ERK inhibitor, attenuates RANKL-induced osteoclast formation and mitigates cartilage inflammation by inhibiting the NF-κB and MAPK pathways. *Bioorg Chem*. 2023;132:106321.
63. Wurm A, Iandiev I, Uhlmann S, et al. Effects of ischemia-reperfusion on physiological properties of Müller glial

Investigative Ophthalmology & Visual Science

cells in the porcine retina. *Invest Ophthalmol Vis Sci*. 2011;52(6):3360–3367.

64. Roth S, Shaikh AR, Hennelly MM, Li Q, Bindokas V, Graham CE. Mitogen-activated protein kinases and retinal ischemia. *Invest Ophthalmol Vis Sci*. 2003;44(12):5383–5395.
65. Yang Y, Wang N, Xu L, et al. Aryl hydrocarbon receptor dependent anti-inflammation and neuroprotective effects of tryptophan metabolites on retinal ischemia/reperfusion injury. *Cell Death Dis*. 2023;14(2):92.
66. Huang S, Huang P, Yu H, et al. Extracellular signal-regulated kinase 1/2 pathway is insufficiently involved in the neuroprotective effect by hydrogen sulfide supplement in experimental glaucoma. *Invest Ophthalmol Vis Sci*. 2019;60(13):4346–4359.

Investigative Ophthalmology & Visual Science